HIGH AREA-TO-MASS RATIO AND SMALL LENGTH-SCALE SPACECRAFT FORMATION FLYING APPLICATIONS

Giorgio Mingotti[(1)], **Colin McInnes**[(2)]
[(1)(2)] *Department of Mechanical & Aerospace Engineering, University of Strathclyde, Glasgow, UK, giorgio.mingotti@strath.ac.uk, colin.mcinnes@strath.ac.uk*

Abstract: *In this paper an analytic formulation of reconfiguration maneuvers for formation-flying is presented. In the framework of the CWH equations, micro-spacecraft with high area-to-mass ratio and small length-scale are considered. As a control strategy, a propellant-free approach is introduced which exploits differential solar radiation pressure by means of electrochromic coating. A new class of space missions is enabled, based on swarms of micro-spacecraft with sensing, computing, bi-directional communicating and micro-power sources. Due to the advances in miniaturized technology, a great number of electromechanical devices can be manufactured and deployed at low cost with active sensors on-board. Taking advantage of the unique geometrical pattern of the arrays of micro-spacecraft enabled by the relative orbital dynamics, the exploitation of Earth remote sensing from Space becomes more accessible to a wider community.*

Keywords: *Relative Motion and Control, Solar Radiation Pressure, Micro-Spacecraft, Electrochromic Control.*

1. Introduction

The last few decades have seen a growing interest in space missions for remote sensing of the Earth. Numerous missions carrying active and passive sensors for military and civil applications have been implemented. Different kinds of sensors are currently available to obtain a complete set of information useful for a plethora of applications (i.e., atmospheric gas monitoring, landslide control, polar ice monitoring, harbour monitoring, etc.). However, due to the elevated overall system complexity of space missions, the raw data products can only be obtained at a relatively high cost. This reduces the diffusion and the exploitation of such raw data, especially for civil applications, where Earth-based solutions often result to be cheaper (i.e., terrestrial monitoring of the environment). The aim of this research is to propose a novel concept of cost effective space missions in order to make remote sensed data accessible to a broader user community.

The recent developments in spacecraft design exploiting miniaturised electromechanical systems with sensing, computing, bi-directional communicating and micro-power functions have enabled a new class of low-cost, low-weight micro-scale spacecraft suitable for use in swarm applications. Current concepts for functional devices in space have been designed by exploiting existing capabilities, such as satellite-on-a-chip [1,2]. Distributed devices for Earth observation and communication, autonomous on orbit self-assembly, diagnostic or environmental detection in the proximity of a large satellite are among the prospective missions that may be enabled. The concept of a swarm of separated elements cooperating coherently enables, for example, the implementation of extremely large aperture radio frequency or optical antennae. These elements would be free-flying in space, either controlled by active or natural forces for each element to stay within a prescribed volume.

The exploitation of orbital dynamics at small length scale and so high area-to-mass ratio requires entirely new techniques for modelling and formation-flying control. Solar radiation pressure and aerodynamic drag may become dominant with respect to the Earth's gravity [3,4]. If the swarm devices are assumed to be coated with an electrochromic material, the relative motion within the formation is controlled via the modulation of differential solar radiation pressure: the optical properties of the elements change when an electrical current is applied [5]. A propellant-free control method is developed to design and maintain the relative orbits of the swarm. The starting point is the linearised formulation of the relative dynamics of the micro-spacecraft flying in close proximity. Assuming they are in low, circular orbits around a spherical Earth in the ecliptic plane, the dynamical model is suitable for generalization and extension to a wider class of orbits that include the main orbital perturbations[6].

Enhanced remote sensing applications - including ionospheric mapping, UWB radar, high resolution and multistatic radar imaging, which have the potential to take advantage of unique geometrical pattern that can be generated by the swarm - can also be investigated as further development of this project. Among them, the concept of synthetic aperture radar and distributed aperture radar appears to be one of the most promising. In particular, applications that include sparse aperture sensing that are able to exploit the synergetic behaviour of the system. The capabilities and the requirements for each of the micro-spacecraft of the swarms to be used as sensor for such applications can be evaluated. For example, since the sensors can be used as antenna array elements (passive or active), two criteria can be used to evaluate the performance and underline the benefit of the swarm architecture: the Point Spread Function (PSF), related to angular resolution, and the Modulation Transfer Function (MTF), related to the sensitivity or contrast characteristic of a filled aperture [7].

This paper is divided into three main Sections: (2.) *Linearized Dynamics*, (3.) *Controlled Dynamics* and (4.) *Test Cases*.

In Section (2.) *Linearized Dynamics*, the relative dynamics of the high area-to-mass ratio and small length scale spacecraft is introduced. The controlled dynamics, based on electrochromic coating that exploits the solar radiation pressure is described in Section (3.) *Controlled Dynamics*, while in Section (4.) *Test Cases*, two types of reconfiguration maneuvers are presented. At the end, Section (5.) *Conclusion*, the final remarks are discussed.

2. Linearized Dynamics

This study introduces the basics to describe the barycentric motion of a swarm of *micro* spacecraft. For sake of clearness in the following formulation, the relative motion dynamics of only two spacecraft in close proximity, named *chief* and *deputy* respectively, traveling around a spherical Earth is considered. It is assumed that the chief flies on a circular low-Earth orbit.

Assuming that the orbital radius of the chief spacecraft is much greater than the relative distance between the spacecraft and considering the *Satellite Coordinate System* (RSW), the linearized relative motion dynamics can be written in the form of the *Clohessy-Wiltshire* or *Hill's* (CWH) equations [8].

$$\begin{aligned} \ddot{x} - 2w_n\dot{y} - 3w_n^2 x &= a_x \\ \ddot{y} + 2w_n\dot{x} &= a_y \\ \ddot{z} + w_n^2 z &= a_z \end{aligned} \tag{1}$$

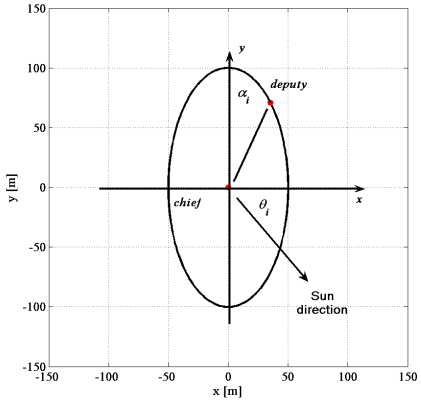

(a) Projected Circular Orbit (PCO) in the $x - y$ plane. The parameter α_i stands for the position of the deputy spacecraft along the periodic orbit, while the parameter θ_i stands for the *in-plane* Sun-direction with respect to the reference frame rotating with the chief spacecraft.

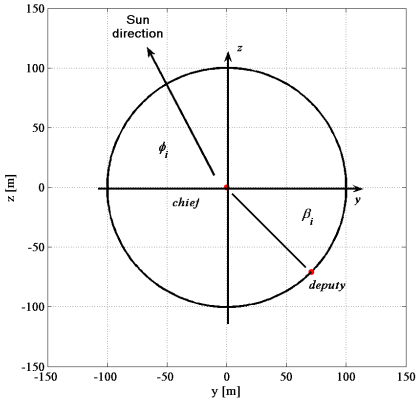

(b) Projected Circular Orbit (PCO) in the $y - z$ plane. The parameter β_i stands for the position of the deputy spacecraft along the periodic orbit, while the parameter ϕ_i stands for the *out-of-plane* Sun-direction with respect to the reference frame rotating with the chief spacecraft.

Figure 1. Relative motion parameters and Sun-direction geometry.

The system of equations written above, when the accelerations $a_x = a_y = a_z = 0$, has an analytic solution of the following form:

$$\begin{aligned}
x(t) &= 4x_i + \frac{2\dot{y}_i}{w_n} + \frac{\dot{x}_i}{w_n}\sin(w_n t) - \left(3x_i + \frac{2\dot{y}_i}{w_n}\right)\cos(w_n t) \\
y(t) &= y_i + \frac{2\dot{x}_i}{w_n} + \frac{2\dot{x}_i}{w_n}\cos(w_n t) + \left(6x_i + \frac{4\dot{y}_i}{w_n}\right)\sin(w_n t) - (6w_n x_i + 3\dot{y}_i)t \\
z(t) &= z_i\cos(w_n t) + \frac{\dot{z}_i}{w_n}\sin(w_n t) \\
\dot{x}(t) &= \frac{\dot{x}_i}{w_n} w_n\cos(w_n t) + \left(3x_i + \frac{2\dot{y}_i}{w_n}\right) w_n\sin(w_n t) \\
\dot{y}(t) &= 6w_n x_i + 3\dot{y}_i - 2\dot{x}_i\sin(w_n t) + (6w_n x_i + 4\dot{y}_i)\cos(w_n t) \\
\dot{z}(t) &= -z_i w_n\sin(w_n t) + \dot{z}_i w_n\cos(w_n t)
\end{aligned} \tag{2}$$

Being interested in a bounded motion, the initial conditions are assumed such that the secular term vanishes (i.e., the coefficient multiplying t). Recalling that orbits are circular, the angular rate w_n is simply the satellite's mean motion:

$$w_n = \sqrt{\frac{\mu_{Earth}}{r_{chief}^3}} \tag{3}$$

where r_{chief} is the radial distance of the chief spacecraft, assuming an orbital altitude of 600 km.

The periodic analytic solutions represented by Eqs. (2) can be re-arranged in a compact

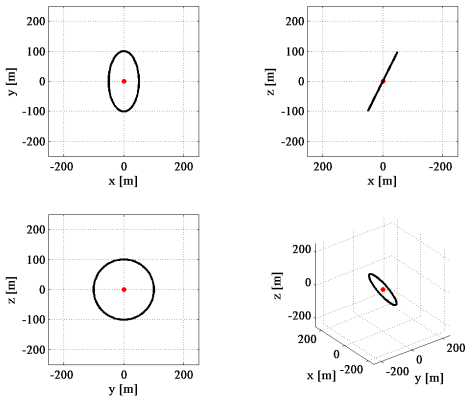

(a) Relative motion configuration, natural dynamics (Projected Circular Orbit (PCO)).

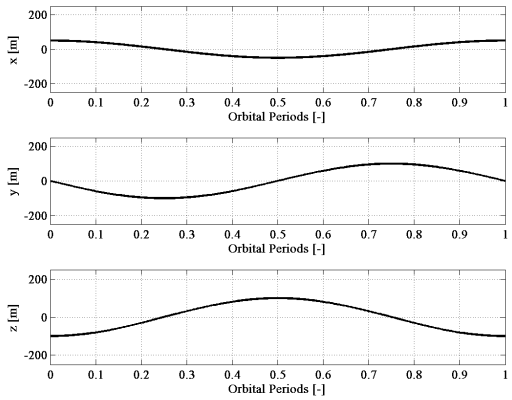

(b) Relative coordinates evolution, natural dynamics (Projected Circular Orbit (PCO)).

Figure 2. Formation-flying relative CWH dynamics.

fashion [9], and a sample Projected Circular Orbit (PCO) is presented in Fig. 2:

$$\begin{bmatrix} x(t) \\ y(t) \\ z(t) \\ \dot{x}(t) \\ \dot{y}(t) \\ \dot{z}(t) \end{bmatrix} = \begin{bmatrix} a_i/2 \; sin(w_n t + \alpha_i) \\ a_i \; cos(w_n t + \alpha_i) + c_i \\ b_i \; sin(w_n t + \beta_i) \\ a_i/2 \; w_n \; cos(w_n t + \alpha_i) \\ -a_i \; w_n \; sin(w_n t + \alpha_i) \\ b_i \; w_n \; cos(w_n t + \beta_i) \end{bmatrix} \tag{4}$$

Depending upon the choice of free-parameters a_i, b_i, c_i, α_i and β_i, relative orbits of various shapes and sizes can be obtained:

- Projected Circular Orbit (PCO) in the $y - z$ plane (see Fig. 1(b));
- General Circular Orbit (GCO) in three-dimensions;
- Leader Follower Configuration (LFC).

The initial parameter a_i stands for the in-plane $x - y$ orbit amplitude, b_i the initial out-of-plane z orbit amplitude, while c_i describes the initial location of the center of the formation along the y axis. Finally, the parameter α_i describes the initial position of the deputy spacecraft along the periodic orbit around the chief in the $x - y$ plane (see Fig. 1(a)), while the parameter β_i describes the initial out of plane position of the deputy spacecraft (see Fig. 1(b)).

3. Controlled Dynamics

In this work a $x - y - z$ spatial configuration has been considered, and only *differential* solar radiation pressure has been investigated as acting perturbation on the system. Therefore the

accelerations read:

$$\begin{aligned} a_x &= +dc_r p_{sr} r_{am} \cos\phi \cos(w_n t + \theta_i) \\ a_y &= -dc_r p_{sr} r_{am} \cos\phi \sin(w_n t + \theta_i) \\ a_z &= +dc_r p_{sr} r_{am} \sin\phi \end{aligned} \tag{5}$$

A few constant appear in Eqs. (5), and they are:

- dc_r: differential reflectivity coefficient;
- p_{sr}: solar radiation pressure, equal to $W/c_{light} = 4.56 \times 10^{-6}$ N/m^2 (with W the energy flux density of the Sun at 1 AU and c_{ligth} the speed of light);
- r_{am}: area-to-mass ratio, equal to 10^1;
- θ_i: Sun-direction (in the $x-y$ plane) with respect of the reference frame rotating with the chief spacecraft (see Fig. 1(a));
- ϕ_i: Sun-direction (in the z axis) with respect of the reference frame rotating with the chief spacecraft (see Fig. 1(b)).

The nominal formation-flying shape investigated is a PCO, where the relative motion is described by a projected circular orbit on the $y-z$ plane.

Thanks to the high area-to-mass ration of the micro-spacecraft taken in consideration, solar radiation pressure reveals to be useful to control the relative motion within the formation in reasonable time. It is assumed that it is possible to change the value of the differential reflectivity coefficient dc_r by means of electrochromic control. Considering that the Sun-facing side of the micro-spacecraft is either completely absorptive ($c_r = 1$) or completely reflective ($c_r = 2$), in this work the chief is assumed to have a reflectivity coefficient $c_r = 1.5$, while the deputy can change its value from $c_r = 1$ to $c_r = 2$ [5]. Therefore, the differential reflectivity coefficient introduced in Eqs. (5) can vary continuously from $dc_r = -0.5$ to $dc_r = +0.5$. Finally, the spacecraft are assumed passively Sun-pointing [10].

Augmenting the original natural system represented by Eqs. (1) with the dynamics of f, that stands for the angular motion along the relative orbit and that has the following analytic solution

$$\left[\ f(t)\ \right] = \left[\ w_n t + \theta_i\ \right] \tag{6}$$

then the controlled dynamical system reads:

$$\begin{aligned} \ddot{x} - 2w_n\dot{y} - 3w_n^2 x &= +dc_r p_{sr} r_{am} \cos\phi \cos(f) \\ \ddot{y} + 2w_n\dot{x} &= -dc_r p_{sr} r_{am} \cos\phi \sin(f) \\ \ddot{z} + w_n^2 z &= +dc_r p_{sr} r_{am} \sin\phi \\ \dot{f} &= w_n \end{aligned} \tag{7}$$

The dynamical system written above admits an analytic solution, assuming that $a_{srp} = p_{sr} \cdot r_{am}$; the x component evolves as follows:

$$\begin{aligned} x(t) \ =& -\frac{1}{12w_n^2} \ (\ -32dc_r a_{srp} \cos\phi \cos(w_n t + \theta_i) + 18dc_r a_{srp} \cos\phi \sin(w_n t) w_n \cos(\theta_i) t + \\ & - 18dc_r a_{srp} \cos\phi \cos(w_n t) w_n \sin(\theta_i) t - 5dc_r a_{srp} \cos\phi \sin(w_n t) \sin(\theta_i) + 24 \cos(w_n t) \dot{y}_i w_n + \\ & - 12 \sin(w_n t) \dot{x}_i w_n - dc_r a_{srp} \cos\phi \cos(w_n t) \cos(\theta_i) - 24 \dot{y}_i w_n + 36 \cos(w_n t) x_i w_n^2 + \\ & + 24dc_r a_{srp} \cos\phi \cos(\theta_i) - 48 x_i w_n^2 + 9dc_r a_{srp} \cos\phi \sin(w_n \, t) \sin(2w_n t + \theta_i) + \\ & + 9dc_r a_{srp} \cos\phi \cos(w_n t) \cos(2w_n t + \theta_i) \ ) \end{aligned} \tag{8}$$

The analytic solution for the y coordinate reads:

$$\begin{aligned} y(t) \ =& -\frac{1}{6w_n^2} \ (\ -30dc_r a_{srp} \cos\phi \sin(\theta_i) - 24 \sin(w_n t) \dot{y}_i w_n + 12 \dot{x}_i w_n - 6 y_i w_n^2 + \\ & - 18 \cos(w_n t) w_n dc_r a_{srp} \cos\phi \cos(\theta_i) t + 18 \sin(w_n t) w_n dc_r a_{srp} \cos\phi \sin(\theta_i) t + \\ & - 5 \cos(w_n t) dc_r a_{srp} \cos\phi \sin(\theta_i) + 18 w_n^2 t \dot{y}_i - 12 \cos(w_n t) \dot{x}_i w_n + \sin(w_n t) dc_r a_{srp} \cos\phi \cos(\theta_i) + \\ & - 36 \sin(w_n t) x_i w_n^2 - 18 w_n t dc_r a_{srp} \cos\phi \cos(\theta_i) + 36 w_n^3 t x_i + 26 dc_r a_{srp} \cos\phi \sin(w_n t + \theta_i) + \\ & + 9 \cos(w_n t) dc_r a_{srp} \cos\phi \sin(2w_n t + \theta_i) - 9 \sin(w_n t) dc_r a_{srp} \cos\phi \cos(2w_n t + \theta_i) \ ) \end{aligned} \tag{9}$$

The z coordinate is expressed as follows:

$$z(t) \ = + \frac{1}{w_n^2} \ (\ \dot{z}_i \sin(w_n t) w_n + z_i \cos(w_n t) w_n^2 + dc_r a_{srp} \sin\phi (1 - \cos(w_n t)) \ ) \tag{10}$$

The $\dot{x}$ velocity evolves as follows:

$$\begin{aligned} \dot{x}(t) \ =& -\frac{1}{12w_n^2} \ (\ 32dc_r a_{srp} \cos\phi \sin(w_n t + \theta_i) w_n - 18 \cos(w_n t) dc_r a_{srp} \cos\phi w_n^2 \cos(\theta_i) t + \\ & - 17 \sin(w_n t) w_n dc_r a_{srp} \cos\phi \cos(\theta_i) + 18 \sin(w_n t) dc_r a_{srp} \cos\phi w_n^2 \sin(\theta_i) t + \\ & - 23 \cos(w_n t) w_n dc_r a_{srp} \cos\phi \sin(\theta_i) - 24 \sin(w_n t) w_n^2 \dot{y}_i + \\ & - 12 \cos(w_n t) w_n^2 \dot{x}_i - 36 \sin(w_n t) w_n^3 x_i - 9 \cos(w_n t) w_n dc_r a_{srp} \cos\phi \sin(2w_n t + \theta_i) + \\ & + 9 \sin(w_n t) dc_r a_{srp} \cos\phi \cos(2w_n t + \theta_i) w_n \ ) \end{aligned} \tag{11}$$

The $\dot{y}$ velocity is expressed as follows:

$$\begin{aligned}\dot{y}(t) \ =&-\frac{1}{6w_n^2}\ (\ -24\cos(w_nt)w_n^2\dot{y}_i + 18\sin(w_nt)dc_ra_{srp}\cos\phi w_n^2\cos(\theta_i)t+\\
&-17\cos(w_nt)w_ndc_ra_{srp}\cos\phi\cos(\theta_i) + 18\cos(w_nt)dc_ra_{srp}\cos\phi w_n^2\sin(\theta_i)t+\\
&+23\sin(w_nt)w_ndc_ra_{srp}\cos\phi\sin(\theta_i) + 18w_n^2\dot{y}_i + 12\sin(w_nt)w_n^2\dot{x}_i+\\
&-36\cos(w_nt)w_n^3x_i - 18w_ndc_ra_{srp}\cos\phi\cos(\theta_i) + 36w_n^3x_i + 26dc_ra_{srp}\cos\phi\cos(w_nt+\theta_i)w_n+\\
&+9\sin(w_nt)w_ndc_ra_{srp}\cos\phi\sin(2w_nt+\theta_i) + 9\cos(w_nt)dc_ra_{srp}\cos\phi\cos(2w_nt+\theta_i)w_n\ )\end{aligned} \tag{12}$$

The analytic solution for the $\dot{z}$ velocity reads:

$$\dot{z}(t) \ =+\frac{1}{w_n^2}\ (\ \dot{z}_i\cos(w_nt)w_n^2 - z_i\sin(w_nt)w_n^3 + dc_ra_{srp}\sin\phi\sin(w_nt)w_n\ ) \tag{13}$$

Finally, the angular coordinate f as function of time reads:

$$f(t) \ = w_nt + \theta_i \tag{14}$$

4. Test Cases

In this section two reconfiguration maneuvers are described. For sake of clearness, only two micro-spacecraft have been considered: the chief, placed in the center of the formation, and the deputy, traveling around the aforementioned spacecraft in a periodic concentric orbit. Both maneuvers take advantage of the analytic formulation of the problem, allowing the maneuver to be solved in closed form as a function of the differential reflectivity coefficient dc_r.

4.1. Relative Orbit Amplitude

A reconfiguration maneuver with the aim of changing the amplitude of a PCO is introduced as first applicative scenario. Starting from an amplitude $a_i = b_i = 100\,\text{m}$, the deputy micro-spacecraft is driven to a larger relative orbit, with an amplitude of $a_f = b_f = 150\,\text{m}$. The initial and final angular positions of the deputy along the periodic relative orbit are assumed as $\alpha_i = \alpha_f = \pi/2$ and as $\beta_i = \beta_f = -\pi/2$. Initially the Sun-direction, in the $x-y$ plane, is aligned with the opposite direction of the transverse axis, i.e. along the $-y$ axis with $\theta_i = \pi/2$, while the out-of-plane Sun-direction angle is $\phi_i = 0.86688\cdot\pi/2$.

The overall reconfiguration is based on four consecutive steps: i) firstly, the active control is applied (for 1/2 orbital periods for 2 orbits) on the deputy spacecraft to move the instantaneous centre of the formation in the positive y direction and to increase the relative orbit amplitude; as the maneuver time is set equal to 2 orbital periods, it is immediately possible to solve Eq. (8) for dc_r, to get the value of the differential reflectivity coefficient necessary to perform the maneuver, $dc_r = 0.31$ in this case. ii) the active control is applied (for 3/4 orbital periods for one orbits) on the deputy spacecraft to move the instantaneous centre of the formation in the positive x direction; once again is it possible to solve Eq. (9) for dc_r, to get the value of the differential reflectivity coefficient required to accomplish the maneuver, $dc_r = 0.36$ in this case.

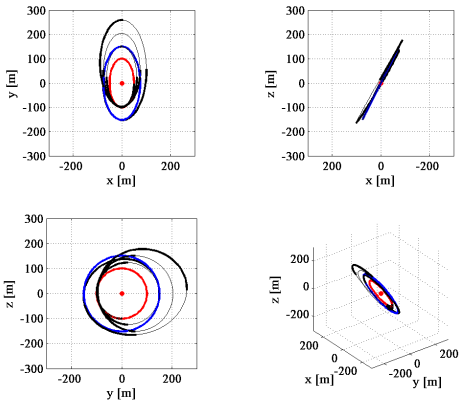

(a) Relative motion configuration, controlled dynamics.

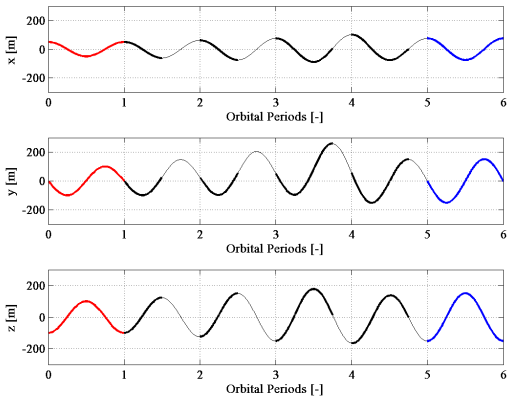

(b) Relative coordinates evolution, controlled dynamics.

Figure 3. Relative orbit amplitude applicative scenario.

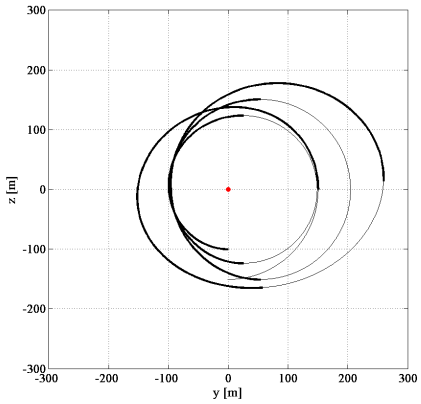

(a) Reconfiguration maneuver.

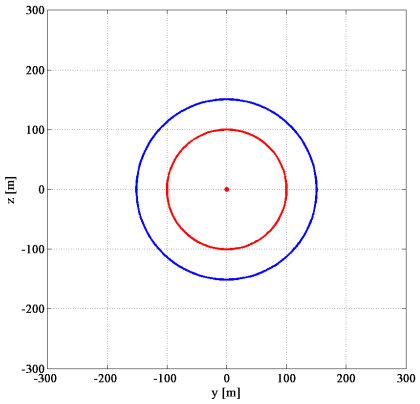

(b) Initial (inner) and final (outer) relative orbits.

Figure 4. Relative motion configuration, $y - z$ plane view.

iii) then, an along-track drift (for 1/2 orbital periods) is achieved and thanks to system natural dynamics the centre of the formation moves along-track (i.e., in the $-y$ direction); iv) finally, an opposite maneuver with respect to the ii) one is performed to cancel the drift and to make the relative orbit periodic around the targeted centre.

Fig. 3(a) describes the motion configuration corresponding to the reconfiguration maneuver aiming at changing the amplitude of the relative periodic orbit. In Fig. 3(b) the relative coordinates are represented, while Fig. 4(a) is the reconfiguration maneuver $y - z$ plane view. In all the plots, the bold lines stand for the trajectory legs where the electrochromic is on duty, while the solid lines represent the system natural dynamics.

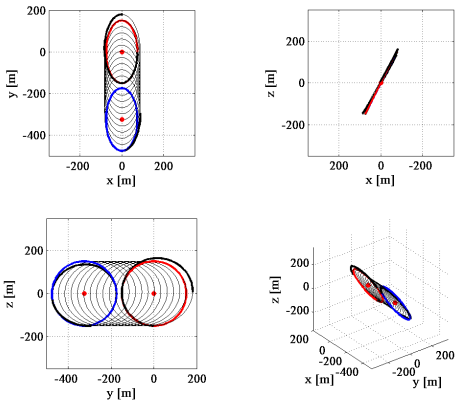

(a) Relative motion configuration, controlled dynamics.

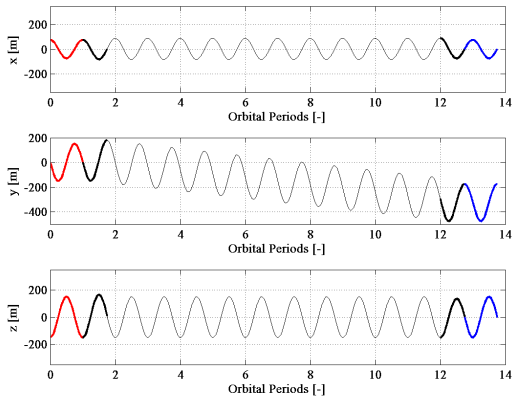

(b) Relative coordinates evolution, controlled dynamics.

Figure 5. Centre shift applicative scenario.

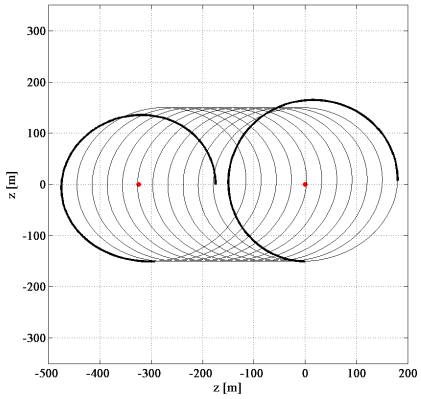

(a) Reconfiguration maneuver.

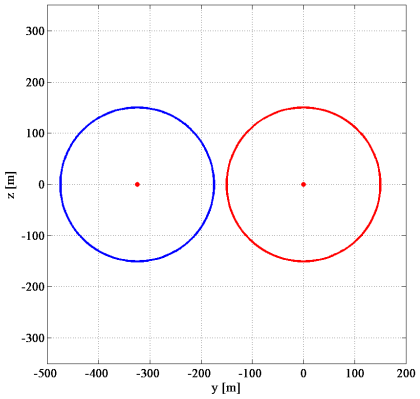

(b) Initial (right) and final (left) relative orbits.

Figure 6. Relative motion configuration, $y - z$ plane view.

4.2. Centre Shift

As second applicative scenario, a reconfiguration maneuver with the aim of shifting the centre of a PCO is described. Starting from an initial location of the centre along the y axis, i.e., $c_i = 0$ m, and with an initial amplitude of $a_i = 150$ m, the deputy micro-spacecraft is driven to a relative orbit, with the same relative amplitude but with a centre location shifted to $c_f = -325$ m.

The initial angular positions of the deputy along the periodic relative orbit are assumed $\alpha_i = \pi/2$, while the final value is set $\alpha_f = 0$ and $\beta_i = \beta_f = -\pi/2$. Initially the Sun-direction, in the $x - y$ plane, is aligned with the opposite direction of the transverse axis, i.e. along the $-y$ axis with $\theta_i = \pi/2$, while the out-of-plane Sun-direction angle is $\phi_i = 0.86688 \cdot \pi/2$.

The overall reconfiguration is based on three consecutive steps: i) firstly, the active control is applied (for 3/4 orbital periods) on the deputy spacecraft to first move the instantaneous

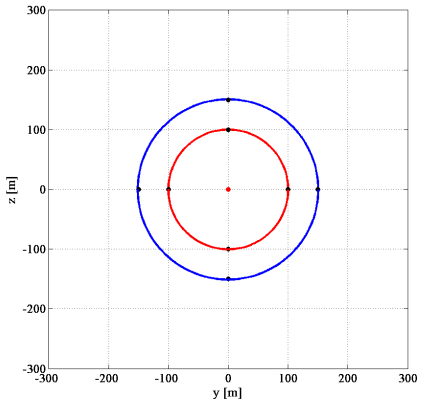

(a) Initial (inner) and final (outer) deputy spacecraft positions.

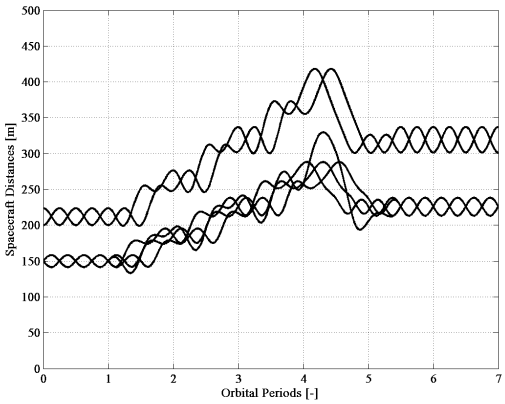

(b) Spacecraft distances during the reconfiguration maneuver.

Figure 7. Multiple spacecraft scenario, configuration and relative distances. Relative orbit amplitude reconfiguration maneuver.

centre of the formation in the positive x direction; ii) then, an along-track drift (for 10 and 1/4 orbital periods) is achieved and thanks to system natural dynamics the centre of the formation moves along-track (i.e., in the $-y$ direction); iii) finally, an opposite maneuver with respect to the initial one is performed to cancel the drift and to make the relative orbit periodic around the targeted centre. Once again is it possible to solve Eq. (9) for dc_r, to get the value of the differential reflectivity coefficient required to accomplish the maneuver, $dc_r = 0.19$ in this case.

Fig. 5(a) describes the motion configuration corresponding to the reconfiguration maneuver aiming at shifting the centre of the relative periodic orbit. In Fig. 5(b) the relative coordinates are represented, while Fig. 4(a) is the reconfiguration maneuver $y - z$ plane view. In all the plots, the bold lines stand for the trajectory legs where the electrochromic control is applied, while the solid lines represent the natural dynamics of the system.

4.3. Multiple Spacecraft

In this section a multiple spacecraft scenario is investigated. Assuming the reconfiguration maneuvers introduced above, formations with 4 deputy spacecraft (uniformly spaced) have been considered. Basically, all the deputy spacecraft fly along the same orbital transfers - described by either Fig. 4(a) orFig. 6(a) - at different times, simply sequentially, i.e. one behind the other.

On the one hand, Fig. 7(a) refers to the maneuver that aims to increase the orbit size of the relative motion, and in particular it describes the position of the 4 deputy spacecraft at the beginning and at the conclusion of the reconfiguration maneuver, while Fig. 7(b) shows the relative distances between the formation spacecraft during the maneuver.

On the other hand, Fig. 8(a) refers to the maneuver that aims to shift the centre of the relative motion: it shows the position of the 4 deputy spacecraft at the beginning and at the conclusion of the reconfiguration maneuver, while Fig. 7(b) describes the relative distances between the formation spacecraft during the maneuver.

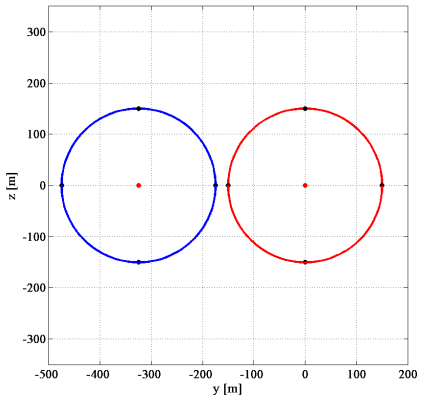

(a) Initial (right) and final (left) deputy spacecraft positions.

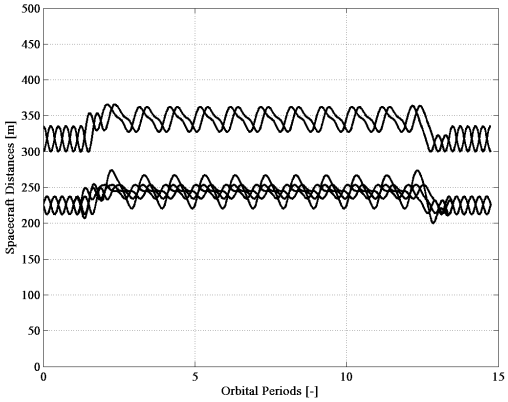

(b) Spacecraft distances during the reconfiguration maneuver.

Figure 8. Multiple spacecraft scenario, configuration and relative distances. Centre shift reconfiguration maneuver.

5. Conclusions

An analytic formulation of reconfiguration maneuvers has been presented in this paper. Two different applicative scenarios have been investigated: change of the orbital amplitude and formation-flying centre shift. Two micro-spacecraft have been considered for sake of clearness during the mathematical formulation of the problem, but the approach has appeared to be easily extended to multiple spacecraft scenarios. The control methods reveals to be propellant-free, as it exploits the differential natural perturbation acting on the system, in detail the solar radiation pressure.

6. Acknowledgements

This research was performed in the framework of the project supported by the European Research Council Advanced Investigator Grant – 227571: VISIONSPACE, Orbital Dynamics at Extremes of Spacecraft Length-Scale.

7. References

[1] Atchison, J. A., and Peck, M., "A Millimeter-Scale Lorentz-Propelled Spacecraft", Proceedings of the AIAA Guidance, Navigation, and Control Conference, Vol. 5, AIAA, Hilton Head, SC, 2007, pp. 5041-5063.

[2] Atchison, J. A., and Peck, M., "Length Scaling in Spacecraft Dynamics", Journal of Guidance, Control, and Dynamics, Vol. 34, No. 1, 2011, pp. 231-246.

[3] Hamilton, D. P., and Krivov, A. V., "Circumplanetary Dust Dynamics: Effects of Solar Gravity, Radiation Pressure, Planetary Oblateness, and Electromagnetism", Icarus, Vol. 123, No.

2, 1996, pp. 503-523.

[4] Colombo, C., and McInnes, C. R., "Orbital Dynamics of 'Smart Dust' Devices with Solar Radiation Pressure and Drag", Journal of Guidance, Control, and Dynamics, Vol. 34, No. 6, 2011, pp. 1613-1631.

[5] Lucking C., Colombo C., McInnes C., "Electrochromic Orbit Control for Smart-Dust Devices", Journal of Guidance Control and Dynamics, 35, (2012).

[6] D'Amico, S., Montenbruck, O., "Proximity Operations of Formation Flying Spacecraft Using an Eccentricity/Inclination Vector Separation", Journal of Guidance, Control and Dynamics, Vol. 29, No. 3, May–June 2006.

[7] Ferretti, A., Monti-Guarneri, A., Prati, C., Rocca, F., Massonet, D., "InSAR Principles: Guidelines for SAR Interferometry Processing and Interpretation ", ESA Publications, February 2007.

[8] Vallado, D., "Foundamentals of Astrodynamics and Application", Second Edition, Kluwer Academic Publishers, 2001.

[9] Vaddi, V., "Modelling and Control of Satellites Formations", PhD Thesis, Texas A&M University, May 2003.

[10] Atchison, J. A., and Peck, M. A., "A Passive, Sun-Pointing, Millimeter-Scale Solar Sail", Acta Astronautica, Vol. 67, No. 1-2, 2010, pp. 108-121.